Coarse-graining for the Analysis of Soft Matter Scattering

submitted by

Andrew R. McCluskey

for the degree of Doctor of Philosophy

of the

UNIVERSITY OF BATH

Department of Chemistry

August, 2018

Declaration of Authorship

I, Andrew R. McCluskey, declare that this thesis titled, "Coarse-graining for the Analysis of Soft Matter Scattering" and the work presented in it are my own. I confirm that:

- where the thesis or any part of the thesis such as a published paper, has been produced jointly with others, that a substantial part is the original work of myself, and
- where the thesis incorporates material already submitted for another degree, the extent of that material and the degree, if any, obtained.

Signed:

Date:

"Atticus told me to delete the adjectives and I'd have the facts."

Scout Finch – To Kill a Mockingbird

UNIVERSITY OF BATH

Abstract

Department of Chemistry

Doctor of Philosophy

Coarse-graining for the Analysis of Soft Matter Scattering

by Andrew R. McCluskey

Acknowledgements

Contents

List of Abbreviations

MD	molecular dynamics
C_{10}TAB	decyltrimethylammonium bromide
DPPC	dipalmitoylphosphatidylcholine
SAS	small angle scattering
GISAS	grazing-incidence small angle scattering
SAXS	small angle X-ray scattering
XRR	X-ray reflectivity
GISAXS	grazing-incidence small angle X-ray scattering
SANS	small angle neutron scattering
NR	neutron reflectivity
GISANS	grazing-incidence small angle neutron scattering
DLS	Diamond Light Source
ESRF	European Synchrotron Radiation Facility
Linac	linear accelerator
BM	bending magnet
rf	radio-frequency cavity
ID	insertion device
ILL	Institut Laue-Langevin
ESS	European Spallation Source
EPSR	emperical potential structure refinement
DWBA	distorted wave Born approximation
PCFF	poly consistent force field
PBC	periodic boundary condition
OPLS	optimized potentials for liquid simulations
NVE	constant number of particles, volume, and energy
NPT	constant number of particles, pressure, and temperature
NVT	constant number of particles, volume, and temperature
WPEP	whole particle effective potential
$C_{10}TANO_3$	decyltrimethylammonium nitrate

Physical Constants

	$\pi = 3.14159\ldots$
Speed of light	$c = 2.998 \times 10^{8}\,\mathrm{m\,s^{-1}}$
Planck's constant	$h = 6.626 \times 10^{-34}\,\mathrm{J\,s}$
Golden ratio	$\Phi = 1.61803\ldots$
Boltzmann's constant	$k_B = 1.380\,648 \times 10^{-23}\,\mathrm{J\,K^{-1}}$

List of Symbols

a_0	optimum head-group area	m^2
b	scattering length	m
b	bond length	m
b_0	equilibrium bond length	m
$c_{\alpha/\beta}$	atom concentrations	m^{-3}
d_n	thickness of layer n	m
f	force	$\mathrm{kg\,m\,s}^{-2}$
f_s	scale factor	
$g_{\alpha\beta}$	partial pair distribution function	
$g(X)$	probability density function	
i	atom type	
k_n	wavevector for layer n	
k_N	dissociation constant from aggregate of N	s^{-1}
l_0	chain length	m
m	mass	kg
n	number of scattering vectors	
n_i	refractive index	
q_i	charge of atom i	k_e
p	surfactant packing parameter	
r_c	cut-off distance	m
r_{ij}	atomic distance	Å
$r_{n,n+1}$	Fresnel equation coefficient	
r_{12}	distance between surfactant centres-of-mass	Å
s	surfactant number	
t	timestep	s
t_F	time-of-flight	s
u	potential energy	$\mathrm{kJ\,mol}^{-1}$
v	velocity	$\mathrm{m\,s}^{-1}$
A	illuminated surface	m^2
$A_{1,2,3}$	dihedral angle parameters	$\mathrm{kcal\,mol}^{-1}$
B	resultant matrix	
C	total solute concentration	$\mathrm{mol\,dm}^{-3}$
C_s	tail carbon atom in surfactant s	
D	number density of particles	m^{-3}
E_k	kinetic energy	J
E_{new}	new energy	kJ
E_{tot}	total energy	kJ
$F(\mathbf{Q})$	diffuse scattering factors	
$G(r)$	radial distribution function	
$I^(Q)$	scattering intensity	cm^{-1}
K	equilibrium constant	
K_b	bond force constant	$\mathrm{kcal\,mol}^{-1}\,\mathrm{Å}^{-1}$
K_θ	angle force constant	$\mathrm{kcal\,mol}^{-1}$

L_F	distance of neutron flight	m
M	layer matrix	
N	aggregation number	$\mathrm{molecule}$
N_{at}	number of atoms	
N_{cycles}	number of cycles	
$N_{\mathrm{particles}}$	number of particles	
N_P	number of undulator magnets	
N_s	head nitrogen atom in surfactant s	
P	probability	
$P(Q)$	particle form factor	
Q	scattering vector magnitude	m^{-1}
R	radius	m
R_g	radius of gyration	m
$R(Q)$	reflectivity	
$Res(Q)$	resolution function	
S	nuclear spin quantum number	
S_a	surface area	m^2
$S(Q)$	system structure factor	
T	temperature	K
T_{inst}	instantaneous temperature	K
$T_{i,f}$	Fresnal transmission factor	
V	volume	m^3
V_c	chain volume	m^3
V_p	particle volume	meter^3
X_N	concentrationof molecules in aggregate of N	$\mathrm{mol\,dm}^{-3}$
$\mathbf{k}_i$	incident wavevector	m^{-1}
$\mathbf{k}_f$	final wavevector	m^{-1}
$\mathbf{r}$	atomic position	
$\mathbf{Q}$	scattering vector	m^{-1}
β	phase factor	
β_c	fraction of c	
$\delta_{\alpha\beta}$	Kronecker δ-function	
ϵ_{ij}	L-J well depth	$\mathrm{kcal\,mol}^{-1}$
θ	polar angle	rad
θ	angle	deg
$\theta_{1/2}$	surfactant-r_{12} angle	deg
θ_c	critical angle	rad
θ_e	electron-photon angle	rad
θ_0	equilibrium angle	deg
λ	wavelength	m
λ_P	magnetic period length	m
μ	atomic mass	amu
μ_N	mean chemical potential of aggregate of N	$\mathrm{J\,molecule}^{-1}$
μ_N°	mean interaction energy of aggregate of N	$\mathrm{J\,molecule}^{-1}$
ν_{samp}	sampling frequency	
ρ	scattering length density	m^{-2}
ρ_0	atomic density	m^{-3}
σ	interfacial roughness	m
σ_i	statistical uncertainty in $I^{\mathrm{exp}}(Q)$	cm^{-1}
σ_{ij}	distance of L-J minima	Å

σ_{coh}	coherent scattering cross section	m^2
σ_{incoh}	incoherent scattering cross section	m^2
ϕ	azimuthal angle	rad
ϕ	dihedral angle	rad
χ^2	chi-squared	
ω	neutron frequency	s^{-1}
ω_i	incident frequency	Hz
ω_f	final frequency	Hz
$\mathrm{d}\sigma/\mathrm{d}\omega$	differential cross-section	m^2
Λ	temperature factor	

1 Theory

1.1 Probing radiation

This work is focussed on the use of X-ray and neutron scattering, therefore it is pertinent to discuss how each of these probing radiation is produced and detail the advantages of each with resepect to the other.

1.1.1 The generation of X-ray and neutrons

X-rays

X-rays are a form of electromagnetic radiation similar to visible light, albeit with a much shorter wavelength – from $0.01\,\mathrm{nm}$ to $10\,\mathrm{nm}$. There are three common ways to produce X-rays; two are available within the laboratory, while the other is exclusive to large scale facilities.

The two laboratory source X-ray generation techniques are the X-ray tube and the rotating anode. An X-ray tube consists of a filament and an anode within a vacuum chamber, by passing a high voltage electrical current across the filament electrons are emitted which accelerate towards the anode. On collision with the anode, the rapid deceleration results in the emission of X-rays of a characteristic wavelength based on the anode material.[1] The most common material for an X-ray tube anode is copper which gives off radiation of about $8\,\mathrm{keV}$.

The other common laboratory method for the generation of X-rays is the rotating anode, which is an improvment on the X-ray tube. In the X-ray tube, each time that an electron contacts the anode there is some energy transfer, this means that over many millions of collisions, the temperature of the anode can raise significantly – leading to a temperature limitation on the X-ray flux available. This lead to the development of the rotating anode, this is simply where the anode is made from a rotating wheel, so that the bombardment is spread across the whole wheel reducing the energy localisation. This allows an increase in the photon flux by about an order of magnitude.[1]

The third method of X-ray generation is at a synchrotron facility, this method has the drawback that it requires access to a national or international faciliy; such as Diamond Light Source (DLS) or the European Synchrotron Radiation Facility (ESRF). The way in which X-rays are generated at the synchrotron involves the acceleration of an electron, rather than the deceleration as with the laboratory sources. This is achieved by having relativistic electrons travel in around a curve, from Newtonian mechanics it is known that travelling on a curve at constant speed is equivalent to acceleration. This is achieved by firstly accelerating the electrons, produced in an linear accelerator (Linac), to near the speed of light in a booster synchrotron before injecting them into the storage ring. In the storage ring, the electrons are kept at relativistic speeds with bending magnets (BM) and straight sections making up a ring (Figure 1.1). The circularity of the ring is dependent on the number of bending magnets that make up the ring; for example, DLS has 48 bending magnets with 48 straight sections.

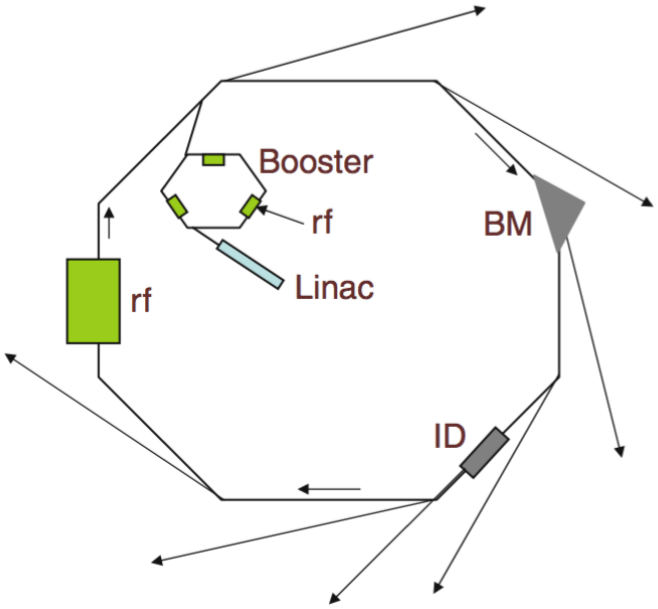

FIGURE 1.1: A schematic representation of a synchrotron radiation source, identifying the Linac, the booster ring, the radio-frequency cavities (rf), the bending magnet (BM) and the insertion device (ID), from Ref [2].

When an electron accelerates (or travels on a curve), Cherenkov radiation is emitted in accordance with the Cherenkov relation,

$$n_i \beta_c \cos\theta_e = 1, \tag{1.1}$$

where, n_i is the refractive index for the dielectric medium, β_c is the fraction of the speed of light at which that electron is travelling, and θ_e is the angle between the electron trajectory and the trajectory of the resulting photon.[2] The curve is the result of a bending magnet, meaning that at each bending magnet there can be a beamline which gives out synchrotron light. The light this is given off from a bending magnet is continuous and broad, covering a wide range of the electromagnetic spectrum. The alternative to a bending magnet beamline is a beamline which is served by an insertion device (ID). An insertion device is able to offer more specific radiation characteristics (photon energy, narrower band) than a bending magnet, and are placed on the magnet-free straight sections of the synchrotron. Common insertion devices include wavelength shifters, wigglers, and undulators.

The type of insertion device that is present at both I07 and I22 at DLS is an undulator. An undulator consists of a series of magnets of opposing polarity whihc causes the electrons to 'wiggle' back and forth (Figure 1.2). This results in a superposition of radition from N_P sources, where N_P si the number of magnets, yielding quasi-monochromatic radiation. The brilliance of different X-ray sources are compared in Table 1.1, this shows the significant benefit that an undulator offers in terms of photon brilliance.

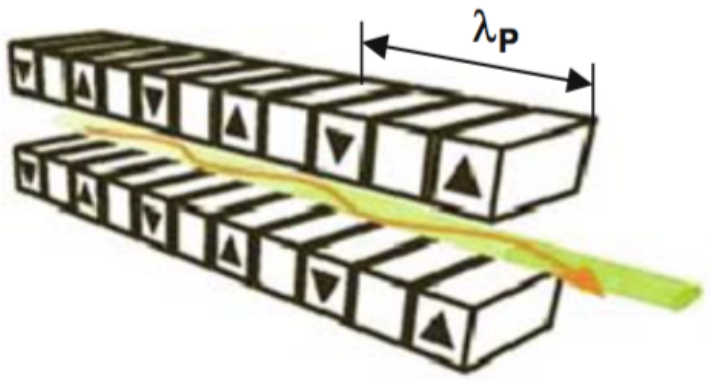

FIGURE 1.2: A diagram of an undulator insertion device such as that on I07 or I22 where λ_P is the period length between opposing magnets, from Ref [2].

TABLE 1.1: A comparision of the photon brilliance from different light sources, adapted from Ref [3].

Light source	Approximate brilliance/ $\mathrm{s}^{-1}\mathrm{mrad}^{-2}0.1\%\mathrm{bandwidth}^{-1}$
Candle	10^5
X-ray tube	10^8
Sun	10^{10}
Bending magnet	10^{15}
Undulator	10^{20}

Neutrons

1.2 Scattering

The use of scattering techniques to probe soft condensed matter systems is commonplace. In this work, we have focussed on the use of small angle scattering (SAS), reflectometry, and grazing incidence small angle scattering (GiSAS) techniques. These are particularly appropriate for application to soft condensed matter systems due to the length scales capable of being probed being similar to the persistence length of the soft condensed matter systems. The length scales covered for such techniques is from around $1\,\mathrm{nm}$ to $100\,\mathrm{nm}$, as is shown in Figure 1.3. Since it is the equilibrium structures(s) under study, there is no interest in the system dynamics. Therefore, the system can be studied using exclusively elastic scattering techniques, where there is no energy transfer between the probing radiation and the system. This is in contrast to inelastic scattering where energy transfer occurs; facilitating the measurement of system dynamics, such as the dynamical modes of polymers of lipid bilayers.[4, 5] The techniques mentioned above all involve the use of elastic scattering and therefore probe the system equilibrium structure.

Both X-ray and neutron scattering techniques are discussed and used in this work. From an experimental viewpoint, there are significant differences between an X-ray scattering and a neutron scattering experiment. However, there is little variation in terms of the data analysis, where the differences are limited to; the nature of the scattering lengths, and the higher background that is present in the neutron scattering experiments.

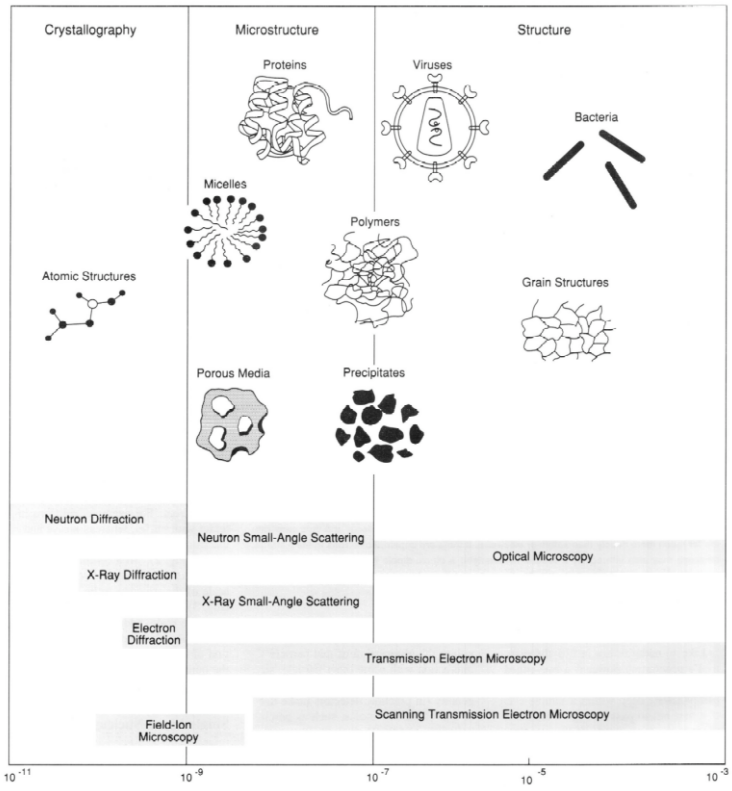

FIGURE 1.3: A representation of how different techniques can be used to probe various length scales, from Ref [3].

1.2.1 The scattering vector

The scattering of some probing radiation, by some sample can be represented as shown in Figure 1.4. Since only elastic scattering is being considered, there will be no change in the frequency of the radiation, $\omega_i = \omega_f$. This means that only the wavevector, $\mathbf{k}$, can change, $\mathbf{k}_i \neq \mathbf{k}_f$. The difference between the incident and final wavevectors is the scattering vector, $\mathbf{q}$, where,

$$\mathbf{q} = \mathbf{k}_i - \mathbf{k}_f. \tag{1.2}$$

The scattering vector strictly has units of m^{-1}, however it is often more practical to use nm^{-1} or $\mathrm{\AA}^{-1}$. Throughout this work, units of reciprocal Ångstrom will be wherever possible. Since the frequency of the probing radiation does not change

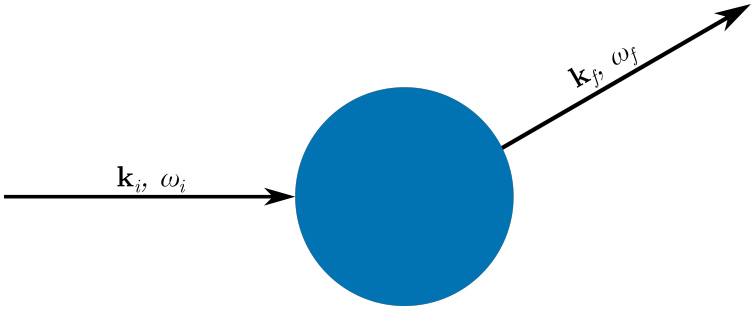

FIGURE 1.4: A schematic of the scattering of some probing radiation by a sample (blue circle), adapted from Ref [3].

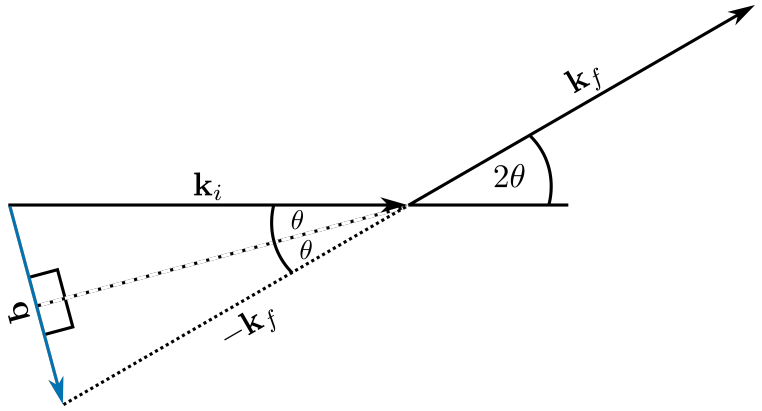

FIGURE 1.5: A vector diagram describing an elastic scattering event, adapted from Ref [3].

during an elastic scattering event, the wavelength, λ, will also not change, meaning that the moduli of the incident and final wavevectors are,

$$|\mathbf{k}_i| = |\mathbf{k}_f| = \frac{2\pi}{\lambda}. \tag{1.3}$$

This means that only the angle will change during the elastic scattering event. The vector diagram in Figure 1.5 can be used to describe the geometry of an elastic scattering event. From this, and Equation 1.3, the value of q, where $q = |\mathbf{q}|$ can be shown as,

$$q = \frac{4\pi \sin\theta}{\lambda}. \tag{1.4}$$

However, this fails to fully capture the three dimensional nature of the scattering event. Hence, it is necessary to describe the scattering with spherical coordinates, 2θ, and ϕ, such that the incoming and outgoing radiation can be described as,

$$\begin{aligned} \mathbf{k}_i &= \left(0, 0, \frac{2\pi}{\lambda}\right), \\ \mathbf{k}_f &= \frac{2\pi}{\lambda}(\sin 2\theta \cos\phi, \sin 2\theta \sin\phi, \cos 2\theta), \end{aligned} \tag{1.5}$$

where, $|\mathbf{k}_f| = {}^{2\pi}/_{\lambda}$. This allows the scattering vector to be written,

$$\mathbf{q} = \frac{4\pi \sin\theta}{\lambda}(-\cos\theta\cos\phi, -\cos\theta\sin\phi, \sin\theta). \tag{1.6}$$

For an isotropic scattering pattern, it is the magnitude of the scattering vector, q, that is measured. In partical terms, the scattering vector allows for easy comparison of measurements made at different radiation wavelengths.

List of Figures

List of Tables

List of Algorithms

Bibliography

[1] H. Schnablegger and Y. Singh, *The SAXS Guide: Getting acquainted with the principles*, Anton Paar GmbH., Graz, Austria, 4th edn., 2017.

[2] M. C. Garcìa-Gutièrrez and D. R. Rueda, in *Applications of Synchrotron Light to Scattering and Diffraction in Materials and Life Sciences*, ed. T. A. Ezquerra, M. C. Garcìa-Gutièrrez, A. Nogales and M. Gomez, Springer-Verlag Berlin Heidelberg, Heidelberg, Germany, 1st edn., 2009, vol. 776, ch. 1, pp. 1–20.

[3] D. S. Sivia, *Elementary Scattering Theory*, Oxford University Press, Oxford, UK, 2011.

[4] V. García Sakai and A. Arbe, *Curr. Opin. Colloid Interface Sci*, 2009, **14**, 381 – 390.

[5] B. Farago, *Curr. Opin. Colloid Interface Sci*, 2009, **14**, 391 – 395.